Phys. Status Solidi A **212,** No. 10, 2332–2340 (2015) / **DOI** 10.1002/pssa.201532405

physica status solidi a
www.pss-a.com
applications and materials science

Thin film solar cell of SnS absorber with cubic crystalline structure

A. R. Garcia-Angelmo, R. Romano-Trujillo, J. Campos-Álvarez, O. Gomez-Daza, M. T. S. Nair, and P. K. Nair*

Instituto de Energías Renovables, Universidad Nacional Autónoma de México, Temixco, Morelos 62580, Mexico

Received 3 June 2015, revised 29 June 2015, accepted 3 July 2015
Published online 28 July 2015

Keywords chemical bath deposition, cubic SnS, thin film solar cell, tin sulfide

* Corresponding author: e-mail pkn@ier.unam.mx, Phone/Fax: +52-55-5622-9742

In a solar cell: stainless steel/SnS/CdS/ZnO/ZnO:Al, we report conversion efficiency of 1.28%, open-circuit voltage (V_{oc}) of 0.470 V, and short-circuit current density (J_{sc}) of 6.2 mA cm^{-2}, measured on cells of area 1 cm^2 under standard conditions. The thin film of SnS absorber of 550 nm in thickness used in this cell was deposited from a chemical bath. Average crystalline diameter of the material is 24 nm, and its X-ray diffraction pattern fits a cubic unit cell with cube edge of 1.159 nm. The optical band gap of the material is 1.74 eV and its electrical conductivity is $10^{-6}\,\Omega^{-1}\,cm^{-1}$. The mobility-lifetime product of the film was determined as 2×10^{-7} cm^2 V^{-1} from photoconductivity measurement. To build the solar cell, a CdS thin film of 50 nm in thickness was deposited from a chemical bath on the SnS thin film prepared on the stainless steel substrate. Subsequently, a ZnO film of 180 nm and ZnO:Al film of 450 nm in thickness were deposited on this CdS defining a solar cell area of 1 cm^2. This solar cell is stable under concentrated sunlight of 2–16 suns, attaining V_{oc} of 0.6 V and J_{sc} of 35 mA cm^{-2} under 16 suns.

1 Introduction The success of CdTe and $CuInGaSe_2$ (CIGS) thin film solar cells have drawn interest toward developing solar cells using alternate "earth-abundant" thin film absorbers [1, 2]. Even though Cu_2ZnSnS_4 or $Cu_2ZnSnSe_4$ solar cells have met with much attention [3], basic attraction in binary compound semiconductors persists because of better control of composition in them rather than in ternary or quaternary compounds. In this respect, SnS thin films either of orthorhombic crystalline structure (SnS-ORT) with optical band gap (E_g) of 1.1–1.3 eV or of cubic structure (SnS-CUB) with $E_g = 1.7$ eV have been investigated as absorbers for solar cells. By mid-2014, solar cells using SnS-ORT reached solar-to-electric energy conversion efficiency (η) of 3.88% and open circuit voltage (V_{oc}) of 0.334 V in solar cells using the absorber films of 1200 nm in thickness prepared by thermal evaporation [4]; and of 4.63% and V_{oc} of 0.39 V using an absorber film of 400 nm in thickness prepared by atomic layer deposition [5]. These solar cells were prepared on Mo-substrates on which the SnS-ORT absorber films were deposited and heat-treated, and Zn(O,S)-In_2O_3:Sn (ITO) thin films were deposited. Solar cells using SnS-CUB absorber films have been reported by us in the cell structure: glass/SnO_2:F/CdS/SnS/C-Ag. These cells gave η of 0.57% and V_{oc} of 0.344 V with a SnS-CUB film of 500 nm in thickness [6]. Solar cell structures combining the two types of SnS films: glass/SnO_2:F/CdS/SnS-CUB/SnS-ORT/Ag reached V_{oc} of 0.37 V and η of 0.2% using SnS-CUB film of 110 nm in thickness and SnS-ORT film of 500 nm in thickness, both prepared by chemical deposition [7].

We report here solar cell prepared on stainless steel (SS) sheet with a device structure: SS/SnS-CUB (550 nm)/ZnO (180 nm)/ZnO:Al (450 nm) with cell area of 1 cm^2. The parameters obtained for this cell are η of 1.28%, V_{oc} of 0.470 V, and a fill factor of 0.44. We describe the performance of the SnS solar cells under concentrated sunlight of 2–16 suns. We also find that the chemically deposited SnS thin film absorber used here to which a crystalline structure of zinc blende was assigned previously might be a simple cube. Overall we place SnS-CUB as a thin film solar cell material, which must be considered along with its polymorph SnS-ORT with distinct characteristics. Together, they offer broader options toward solar cell designs.

2 Experimental Substrates: Thin films of SnS were deposited on either Corning microscope glass substrates 25×75 mm^2 of 1 mm thickness or on commercial SS substrates (of 0.8 mm in thickness of mirror finish) cut to

the same area. SS substrates were immersed in dilute HCl (diluted to 50% of as-supplied conc. HCl) for 6 min at room temperature. This changed the reflective mirror-like surface of Cr-steel to a relatively rough surface by leaching the top oxide layer. Glass substrates were washed in neutral soap solution, rinsed in distilled water, and dried. Glass and SS substrates were immersed in a dilute Na_2S solution of 0.03 M concentration for 12 h at room temperature to activate the surface. This surface treatment was reported previously for chemically deposited SnSe thin films [8]. The substrates were rinsed in distilled water and dried prior to SnS deposition.

2.1 Deposition of SnS thin films A 0.1 M solution of Sn (II) was prepared by heating with stirring 2.26 g of $SnCl_2 \cdot 2H_2O$ (Aldrich) in 30 mL of glacial acetic acid and 1 mL of concentrated HCl. De-ionized water was added to this mixture to take the final volume to 100 mL. To 10 mL of this solution taken in a beaker, were added 30 mL of 3.7 M triethanolamine, 16 mL of 30% NH_3 (aq.), and 10 mL of 0.1 M thioacetamide. The final volume was taken to 100 mL with de-ionized water. Baker-Analyzed reagents were used. Clean microscope glass slides or SS substrates were supported vertically on the beaker-wall. After 10 h inside this bath at 17 °C, the substrates were removed and rinsed in de-ionized water. The film is of thickness 150 nm, as determined by step-measurement using Ambios-XP200. In three more depositions in freshly prepared baths, the film thickness was increased to 550 nm. Film from one side of the substrates was removed using cotton swabs moistened in dilute HCl. The Sn(II) solution prepared as described above would produce compact, specularly reflective films if chemical bath deposition is done within 4 days.

2.2 Development of solar cells Thin film of CdS of 50 nm in thickness and of predominantly hexagonal crystalline structure was deposited on SS/SnS (550 nm) at 80 °C in 30 min, using a chemical deposition bath using cadmium–citrate complex and thiourea, reported in 1994 [10]. Using Teflon sealant tapes four areas of 1×1 cm^2 each were opened on the SS/SnS/CdS film surface. These substrate/film structures were mounted on a rotating substrate holder of a radio frequency (r.f.) magnetron sputtering unit, which uses dual 7.8 cm (3-inch) ZnO and ZnO:Al targets (Kurt Lesker). The sputter deposition was done at r.f. power of 180 W and 6 mTorr of argon pressure. During 30 min of deposition, a ZnO film of 180 nm in thickness was deposited first. Subsequently a ZnO:Al film of 450 nm in thickness was deposited in 30 min on the ZnO film using r.f. power of 280 W at a pressure of 2 mTorr. Figure 1(a) shows the scheme for this cell and (b) shows the photograph of four cells of area approximately 1 cm^2 each on the stainless steel substrate. X-ray diffraction (XRD) and optical reflectance studies were done on the cell at this stage. Flexible PVC-clad multi-strand copper cable was fixed to the ZnO:Al film on each cell using silver-epoxy paint, as illustrated in Fig. 1(c). The active (non-shaded area) of the cell is typically 95%; for J_{sc} estimation area of the cell is considered as 1 cm^2.

2.3 Characterization XRD studies were made on the SnS film deposited on the glass substrate at grazing incidence (δ) of 1.5° and on the cell structure in the θ–2θ mode. Rigaku D-Max 2200 diffractometer with CuK_α radiation was used for this study. Optical transmittance (T) and reflectance (R) measurements on the film were made for film-side incidence with air and front-aluminized mirror, respectively. Diffuse reflectance measurement was made on the cell structure to estimate the optical absorptance and the maximum photogenerated current density (J_L). For the measurement of photocurrent response of the film on glass substrates, two silver paint electrodes of 5 mm length at 5 mm separation were applied on the film surface. Keithley 690 multimeter and 230 Programmable voltage source were interfaced to a computer to record dark and photocurrent levels during 20 s dark–20 s light–20 s dark. Illumination intensity of 1000 W m^{-2} from a tungsten halogen lamp was used for illumination during "light." This measurement was also made using monochromatic light provided through an interference filter to help estimate the mobility-lifetime product of photogenerated charge carriers. Solar cell characteristics were recorded in the interior at 25 °C using a Sciencetech (Canada) photovoltaic testing system (PTS) utilizing a xenon lamp and filters to set the illumination at air-mass AM 1.5 Global solar spectrum at an intensity of 1000 W m^{-2}. For the measurement of external quantum efficiency of the solar cell, a Sciencetech PTS-2-171 using a chopper and lock-in amplifier system was used. The V_{oc} and short-circuit current (I_{sc}) of the cells were also measured directly under concentrated solar radiation at mid-day with solar radiation intensity at 950–980 W m^{-2} at concentrations of 1–16 suns. Values for J_{sc} in this case were normalized for an intensity of 1000 W m^{-2} (one sun) and cell area 1 cm^2. Concentrated sunlight was delivered to the cell using a glass lens of 8.7 cm in diameter, taking into account the reflection and absorption losses in the glass lens following a methodology described previously [11]. The measurement set up is illustrated in Fig. 1(d). The concentration of sunlight was varied by changing the position of the cell along the vertical axis. By opening a shutter momentarily, V_{oc} and I_{sc} were recorded at an ambient temperature of 26–28 °C without allowing the cell temperature rise. The J–V characteristics were also measured using a home-designed curve-tracer for illumination up to 4.3 suns in about 10 s. Measurements at still higher intensities caused the cell temperature to rise and are not reported here.

3 Crystalline structure of SnS thin film The commonly reported crystalline structure for SnS is orthorhombic. However, thin films of SnS of rock salt (RS) or zinc blende (ZB) structure in cubic (CUB) system are also known. Thin films formed by thermal evaporation on NaCl crystal take up the RS-structure with $a = 0.600$ nm [12], whereas nanocrystals formed at 170 °C from an oleylamine preparation of $SnCl_2$ and elemental S has been classified under SnS-ZB with $a = 0.5845$ nm [13]. Thin films of SnS obtained at a temperature of 20–25 °C using the

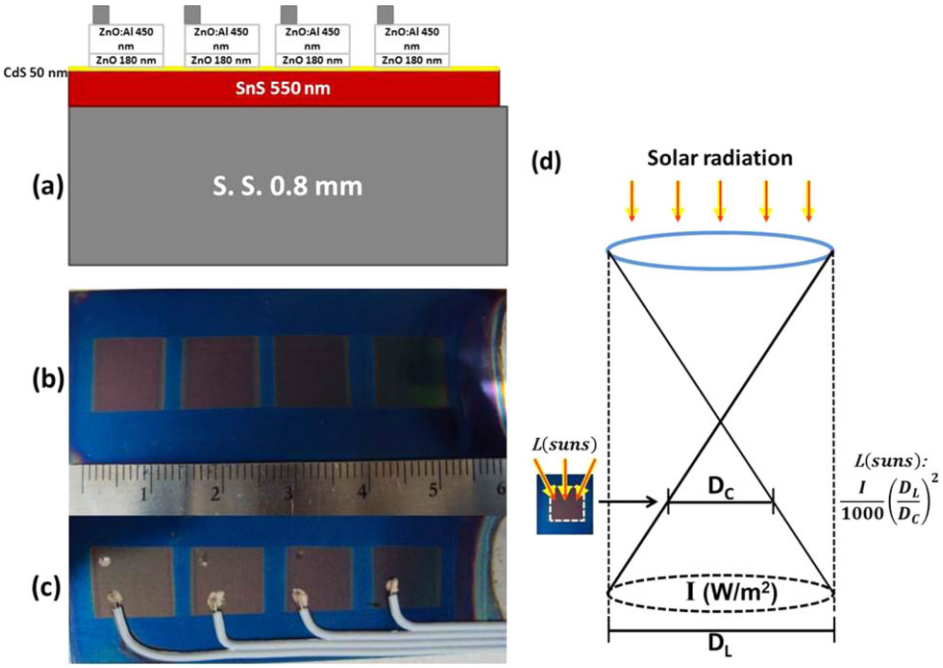

Figure 1 (a) Cross-sectional scheme of the SS–SnS(CUB)–CdS–ZnO–ZnO:Al solar cell structure; (b) photograph of four solar cells, each of area approximately 1 cm^2 developed on a SS-sheet of 2.5×7.5 cm^2 on which the GIXRD and optical reflectance measurements were made; (c) finished solar cells with multi-strand copper wire fixed to them using colloidal silver paint; and (d) measurement scheme for the solar cell in the exterior under concentrated sunlight of 1–16 suns.

chemical formulation for the deposition bath used here were classified as "polymorphic" with predominantly SnS-ZB component in the films with $a = 0.5783$ nm, but with the inclusion of components assigned to SnS-OR as well [9]. Subsequently SnS-ZB was reported for the films obtained at pH 5 in chemical bath deposition but the deposition produced SnS-ORT film if pH was increased to 6 [14]. We observed that in a chemical bath deposition method originally developed for SnS-ORT films [15, 16], SnS-ZB is the dominant crystalline phase in the film when it is deposited at 20–30 °C. Only at temperatures above 35 °C, SnS-ORT phase takes over in the film [17]. There exists uncertainty in assigning to the material either RS or ZB crystalline structure. The reason is that both are of face centered cubic lattice: for $a = 0.600$ nm [12] or 0.580 nm as in PDF-77-3356 for SnS-RS, or for $a = 0.5845$ nm for SnS-ZB nanocrystals [13] or of 0.5783 nm in thin films [9]. The distinguishing feature between the ZB and RS diffraction patterns is in the relative intensities of diffraction from all-odd or all-even (*hkl*) planes. For SnS-ZB, the diffraction peak from (111) planes appearing at 2θ of nearly 26.5° will be stronger than that from (200) planes at 2θ near 31°, and vice versa in SnS-RS [18]. However, preferential orientation of (200) planes in ZB or of (111) planes in RS could reverse such intensity differences in thin films, and make such "ZB-RS"-distinction difficult. Density functional theory (DFT) calculation suggests that SnS-ZB is not thermodynamically stable. Values obtained for $a = 0.643$ nm [18] or 0.66 nm [19] are both nearly 10% above the experimental value of nearly 0.58 nm for SnS-ZB [9, 13]. These studies found that for SnS-RS, the theoretical models offers a value for $a = 0.58$ nm, which is close to the experimental values. The energy–volume curve has a minimum of zero at this value of a, thereby ascribing it thermodynamic stability [18]. Irrespective of the exact implication of thermodynamic instability of SnS-ZB, its crystalline structure is found intact in thin films heated in a nitrogen atmosphere at temperature of 350 °C [9]. In order to account for these disparities, a pseudo tetragonal crystal structure with $a = 1.155$, $b = c = 0.412$ nm has been suggested [19] as a modification of SnS-OR ($a = 1.118$ nm, $b = 0.398$ nm, and $c = 0.433$ nm). A simple cubic cell structure with $a = 1.17$ nm is seen to account for the electron diffraction patterns on nanocrystals of SnS, which is the latest addition to the endeavors for structural assignments in SnS [20].

In Fig. 2(a) is presented the XRD pattern measured at $\delta = 1.5°$ for the film of 550 nm in thickness deposited on glass and in Fig. 2(b), that for the SS/SnS/CdS/ZnO/ZnO:Al cell structure, measured in the θ–2θ mode. The average crystalline grain diameter evaluated from the half-width of the prominent diffraction peaks is 24 nm. In both the patterns, the peak intensity assigned to diffraction from SnS (111) planes at $2\theta = 26.6°$ is nearly the same as that for diffraction from its (200) planes at 2θ of 30.8°. Based on the positions of these peaks, a lattice constant $a = 0.5796$ nm may be assigned for a cubic cell. This result matches those reported previously for SnS-ZB nanocrystals [13] or for thin films [9, 14, 17]. The PDF 77-3356 given here is of

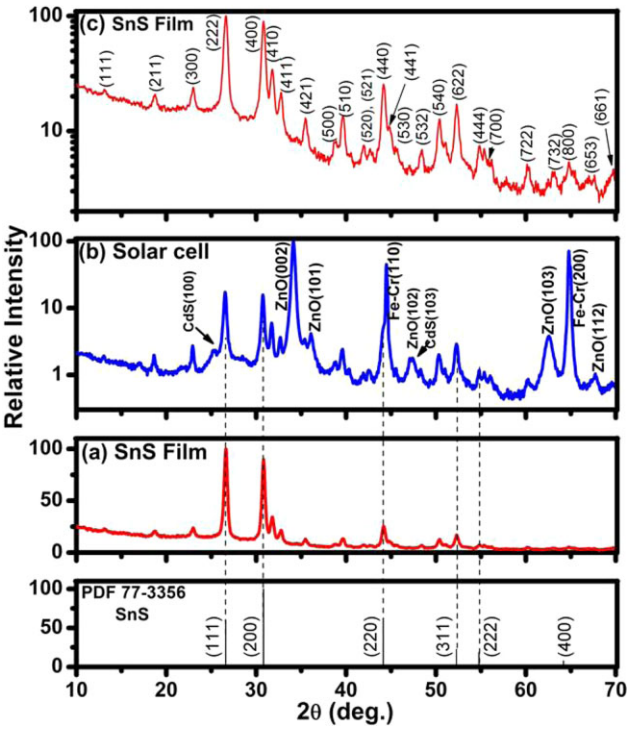

Figure 2 Bottom strip: relative intensities for crystalline planes of cubic SnS of rock salt structure reported in PDF 77-3356; (a) GIXRD pattern recorded at $\delta = 1.5^{\circ}$ for SnS film of 550 nm in thickness deposited on glass substrate with positions of major peaks matching those in the PDF; (b) XRD pattern with intensity on log-scale of the solar cell structure showing the diffraction peaks corresponding to SnS, ZnO (PDF 36-1451), hexagonal CdS, and to SS-substrate (PDF 34-0396 for Fe-Cr); (c) diffraction pattern of (a) plotted on a log-scale, showing that all the diffraction peaks may be assigned to (*hkl*) planes if a unit cell of cube edge 1.1592 nm is taken as the basic building block of this SnS thin film.

SnS-RS (the only available PDF for SnS-CUB in our library) for which diffraction from (111) planes is weaker (60%) compared to that from (200) planes [18]. While all observed diffraction peaks in the XRD pattern in Fig. 2(a) and (b) do not pertain to the cubic structure, the major ones do so. In view of the recent work on SnS nanocrystals [20], we considered here a cubic cell of $a = 2 \times 0.5796$ nm (1.159 nm), which is twice that for the SnS-ZB obtained as above. In this study, we did not yet assign the atomic positions of all 64 atoms in this large cubic cell, eight times as large as the SnS-ZB to which it was thought to belong. In order to consider (*hkl*) assignment to all the observed peaks, the XRD pattern for the film in Fig. 2(a) is re-plotted in a log-scale in Fig. 2(c). We find that all the diffraction peaks for the SnS thin film can be assigned to specific (*hkl*) planes. Further analysis based on this new crystalline structure [20] is in progress for the films that were initially reported from our group as SnS-ZB [9, 17]. Based on the present findings, we classify henceforth the crystalline structure of the absorber film as "SnS-CUB" to signify the simple cubic structure. The deposition of the SnS films on glass or SS substrates does not lead to any notable difference in 2θ positions or relative intensities among the XRD peaks. Peaks other than those belonging to SnS-CUB in the XRD pattern in Fig. 2(b) are assigned to CdS, ZnO, and the stainless steel (Fe-Cr) substrate, with the crystalline planes labeled according to PDF 41-1049 for CdS-hexagonal, PDF 36-1451 for ZnO, and PDF 34-0396 for Fe-Cr.

4 Optical band gap of SnS-CUB thin film In Fig. 3(a) are given the optical transmittance (T) and reflectance (R) spectra of the SnS-CUB film. The optical absorption coefficient (α) of the material for photon energy ($h\nu$) has been evaluated by considering multiple reflections in the film as described in Ref. [21], and is plotted in Fig. 3(b). Figure 3(c) describes the analysis of the electronic transition and type of the band gap. A straight line fit for $(\alpha h\nu)^{2/3}$ versus $h\nu$, in the photon energy range 1.85–2.25 eV suggests forbidden electronic transitions across a direct band gap. From this plot, a value for E_g of the material is determined as 1.74 eV (direct-forbidden). This is the same value for E_g as reported by us previously for this material [9] and within the range of 1.66–1.75 eV reported for SnS-CUB by other chemical deposition methods [14, 17]. The value for E_g obtained here for SnS-CUB is substantially greater than that for SnS-ORT, which has an indirect-E_g of 1.076 and 1.049 eV or a direct-E_g of 1.296 eV reported in a theoretical–experimental work [22] and frequently mentioned in the literature [17]. There is a tail region in the $(\alpha h\nu)^{2/3}$ versus $h\nu$ plot of Fig. 3(c), suggesting the onset of the optical absorption at photon energy 1.69 eV. This arises from an experimental limitation, due to minor differences from an exact match of the maxima and

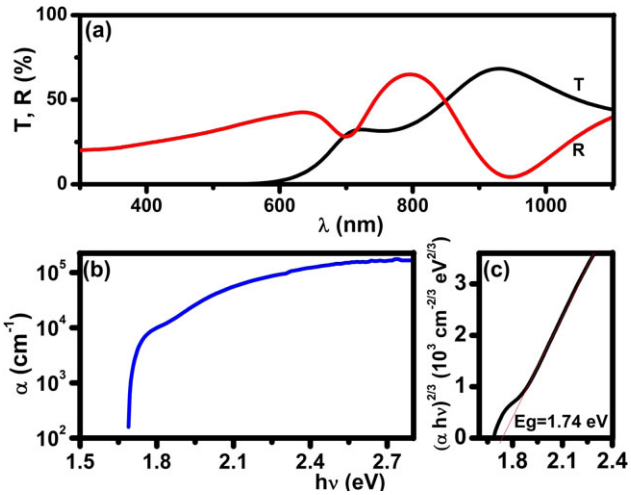

Figure 3 (a) Optical transmittance (T) and specular reflectance (R) of SnS-CUB thin film of 550 nm in thickness; (b) variation of optical absorption coefficient (α) of the film with photon energy ($h\nu$); (c) analysis of the type of electronic transition and optical band gap.

minima of the T and R spectra, because, T is measured at normal incidence and R, at 5°.

5 Light-generated current density Having a larger optical band gap of 1.74 eV in SnS-CUB compared with that of SnS-ORT ($E_g = 1.1$–1.3 eV) would limit the maximum conversion efficiency for solar energy to electricity to less than 30%; for SnS-OR it would be near the maximum possible of 31% predicted for a semiconductor with E_g of 1.3 eV [23]. The light generated current density J_L in SnS-CUB when it functions as the sole-optical absorber in a solar cell may be estimated as a function of the film thickness (d), as illustrated for many semiconductors [24]. Such J_L approximates well with J_{sc} in well-designed solar cells: of nearly 28 mA cm^{-2} for CdTe, and 42 mA cm^{-2} for $CuInSe_2$ or Si. This estimation uses the spectral distribution of the photon flux density, $N_{ph}(\lambda)$ for AM 1.5 G solar spectrum and values of $\alpha(\lambda)$ analogous to $\alpha(h\nu)$ plot given in Fig. 3(b). The method assumes that there is no reflection loss; that $\alpha(\lambda)$ and E_g do not vary with thickness and also that quantum efficiency (QE) for incident photons with $h\nu > E_g$ for electron–hole pair generation is unity. Multiple electron–hole pair generation may occur for $h\nu > 4\,E_g$, but its overall contribution to J_L and hence to J_{sc} of solar cells may be less than what was originally expected [25]. Figure 4(a) shows the results for SnS-CUB, in which the J_{Lmax} for the film with large thickness is 24.5 mA cm^{-2}. For SnS-CUB absorber of 550 nm in thickness used in the present solar cell structure, J_L is 18.7 mA cm^{-2}. In the actual solar cell, reflection losses (R) must be considered as given in Fig. 4(b). Optical absorption ($A = 1 - R$) occurring in the wavelength interval between the threshold of optical absorption in the ZnO:Al/ZnO and in SnS-CUB would create electron–hole pairs in the solar cell and contribute to the current density. Thus, even though AM 1.5 G solar radiation shows on to the cell a photon flux of nearly 4.2×10^{21} m^{-2} s^{-1} as shown in Fig. 4(c), only a fraction of this, 1.14×10^{21} m^{-2} s^{-1}, is captured in the SnS-ZB absorber film, as illustrated in Fig. 4(d). For QE of unity in a solar cell, this photon flux would provide a J_L of 18.2 mA cm^{-2}. In the case of thin film solar cells using SnS-ORT absorber J_L would reach 42 mA cm^{-2} [4]. For SnS-CUB absorber film of E_g 1.74 eV, the trade-off in J_{Lmax} must bring-in a V_{oc} more than that reported using SnS-ORT absorber. An option to combine SnS-ORT with SnS-CUB has been tried previously but without notable advantage [7].

6 Photoconductivity of the SnS film Figure 5(a) shows the photoconductivity response of SnS-CUB thin film. The black-line plot shows that the electrical conductivity in the dark (σ_d) of the material is $0.22 \times 10^{-6}\,\Omega^{-1}$ cm^{-1} which increases to a photoconductivity (σ_p) of $3.4 \times 10^{-6}\,\Omega^{-1}$ cm^{-1} under an intensity of illumination of 1000 W m^{-2} (tungsten–halogen lamp). The photoconductivity response was also measured under near-monochromatic illumination using a narrow-band pass interference filter for a wavelength

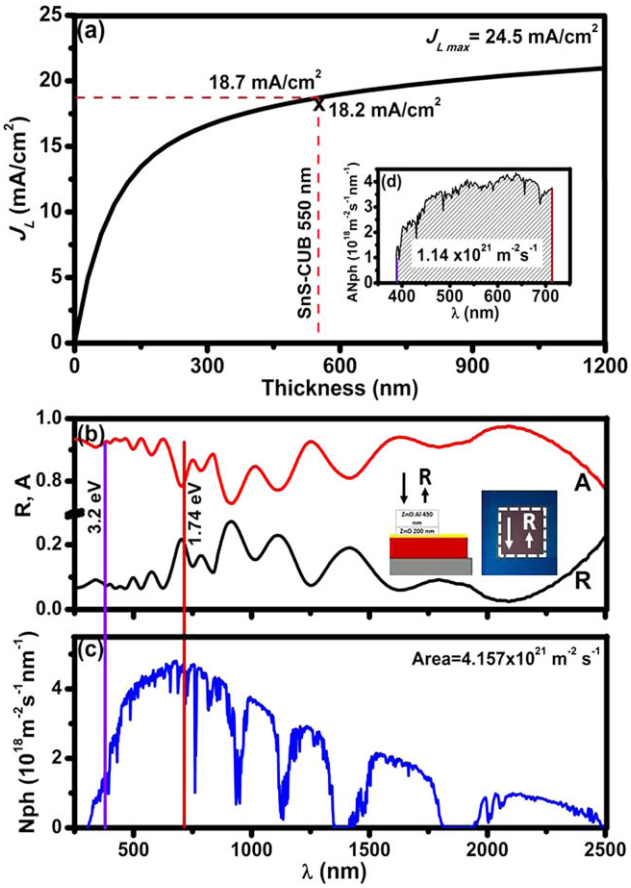

Figure 4 (a) Estimate for photogenerated current density (J_L) for SnS-CUB absorber film of different thicknesses showing a maximum ($J_{L\,max}$) of 24.5 mA cm^{-2} for large thickness and 18.7 mA cm^{-2} for a thickness of 550 nm; (b) optical reflectance (R) and absorptance (A) of the solar cell showing the spectral region in which the SnS thin film will absorb photons from A.M. 1.5 G solar spectrum; (c) spectral distribution of photon flux density for A.M. 1.5 G solar radiation; (d) absorbed photon flux of 1.14×10^{21} m^{-2} s^{-1} producing J_L of 18.2 mA cm^{-2}.

of 600 nm. The optical transmittance of 0.25 (25%) of the filter is centered at this wavelength with a full-width at half maximum of 11 nm. The filter provides on the sample plane a narrow band of photon flux density originating from the tungsten–halogen lamp. This lamp has a spectral distribution of photon flux density $N_{ph}(\lambda)$ given in Fig. 5(b). The quantity $G(\lambda) = [N_{ph}(\lambda)T_{Filter}A_{Film}]/d$ is the spectral distribution of photon flux density absorbed in the film (of thickness $d = 550$ nm), as given in Fig. 5(d). Values of $A_{Film} = (100 - T - R)/100$ are obtained from Fig. 3(a) and T_{Filter} is measured in the spectrophotometer. Both of these are presented in Fig. 5(c). Under QE = 1 and in the approximation of uniform optical absorption of photons, the volumetric generation rate of electron–hole pairs in the SnS-CUB film is $G = 9.8 \times 10^{24}$ m^{-3} s^{-1}. This value is obtained from the shaded area in Fig. 5(d). This generation causes the increase in the electrical conductivity ($\Delta\sigma$)

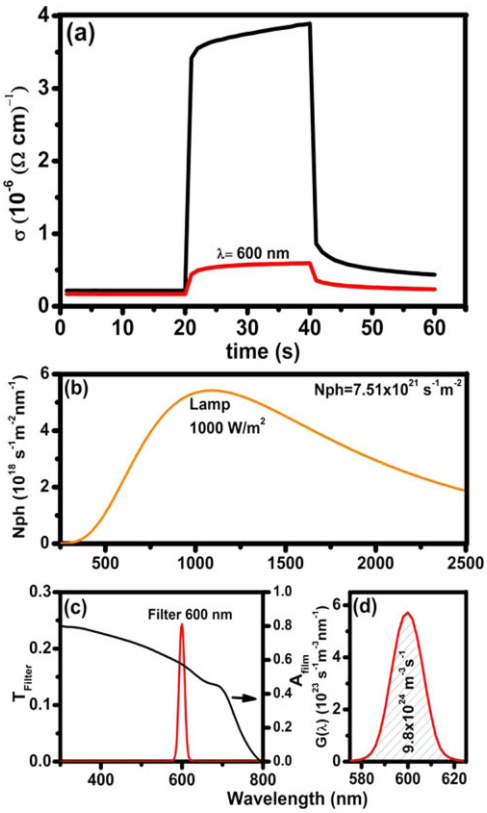

Figure 5 (a) Photoconductivity response of the SnS-CUB film at an illumination intensity of 1000 W m^{-2} of tungsten halogen light (dark line) and under monochromatic illumination provided through an interference filter for wavelength 600 nm; (b) spectral distribution of photon flux density for the tungsten–halogen lamp; (c) optical transmittance of the filter (T_{Filter}) and absorptance of the film (A_{Film}); (d) volumetric absorption rate of photons 9.8×10^{24} m^{-3} s^{-1} in the film during the photoconductivity response measurement resulting in the red line curve in (a).

of $0.3 \times 10^{-6}\,\Omega^{-1}\,\text{cm}^{-1}$ recorded at 1 s as seen from the red curve in Fig. 5(a). This increase is related to other material parameters as: $\Delta\sigma = qG\tau\mu$, where q is the electronic charge, τ is the free-carrier life time, and μ is charge carrier drift mobility. Thus, the mobility-lifetime product ($\mu\tau$) for the photo-generated carriers in the SnS-CUB is $2 \times 10^{-7}\,\text{cm}^2\,\text{V}^{-1}$. A value for μ could not be determined in this work because of the high resistance of the SnS-CUB film. If we assume that it is in the interval of 10–100 cm^2 V^{-1} s^{-1}, then τ would have a value of 2–20 ns. We may note that the hole-mobility reported for SnS-ORT is 90 cm^2 V^{-1} s^{-1} [26] and in a device modeling for SnS-ORT solar cells, electron mobility of 30 cm^2 V^{-1} s^{-1} and hole mobility of 10 cm^2 V^{-1} s^{-1}were considered [27]. However, SnS-CUB is a semiconductor distinct from SnS-ORT, and hence mobility values cannot be borrowed. In order to draw a comparison of τ estimated as described above, we note that in $CuInGaSe_2$ absorber film constituting a thin film solar cell of η of 18%, τ is >100 ns, whereas in $Cu_2ZnSnSe_4$ film used in a solar cell of η of 9%, it is just 2 ns [3]. Heat processing of the film improves the crystalline grain diameter, carrier life time, and hence solar cell performance in SnS-ORT [5]. Device modeling suggests that a lifetime of 1 ns could lead to an efficiency of 10% [27]. Such study has not yet been done for SnS-CUB.

7 Solar cell characteristics Figure 6 shows the *J*–*V* characteristics of the cell described in Fig. 1(c) measured under standard conditions in the interior using simulated AM 1.5 G illumination of intensity 1000 W m^{-2} in the photovoltaic testing system. The parameters listed here are those given by the software of the measurement system. Independent outdoor measurements were also made, as described below. Notable characteristics of the solar cell are $V_{\text{oc}} = 0.470$ V and $\eta = 1.28\%$ for the cell of area 1 cm^2. Values of V_{oc} for solar cells using SnS-ORT are usually below 400 mV [4, 5]. Most device models for CdS/SnS-ORT junctions [28–30] have come to the same conclusion that there is a large conduction band offset at the semiconductor interface and hence there exists a need for an n-type buffer layer with an electron affinity numerically less than that of CdS. In SnS-ORT solar cells, the use of Zn(O,S) [29] or $Zn_{1-x}Mg_xO$ [31] buffer layers, helped η reach 2% in 2013, which was not possible with CdS layers. The oxide layers between the interface and ZnO n-layer was considered vital toward increasing η to 3.88–4.63% in 2014 [4, 5]. In this work, we noted that the absence of CdS layer in the device structure between the SnS-CUB absorber and ZnO affects the solar cell parameters adversely. After an initial trial, such device was dropped from this study.

A V_{oc} of 470 mV of the solar cell using an SnS-CUB absorber given here is among the highest reported for SnS thin film solar cells, but its J_{sc} of 6.2 mA cm^{-2} is only one-third of 18.2 mA cm^{-2} predicted from the analysis of J_{L} in Fig. 4(a). One reason for this shortfall is the short free carrier life time of 2–20 ns estimated from the photoconductivity. Figure 7 shows the external quantum efficiency (EQE) plot for the cell, given along with the optical transmittance of

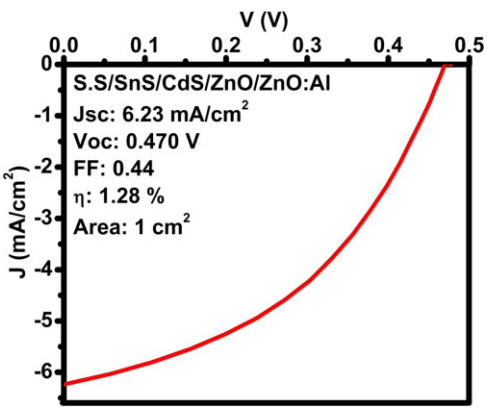

Figure 6 *J*–*V* characteristics of the solar cell measured in the interior under standard conditions.

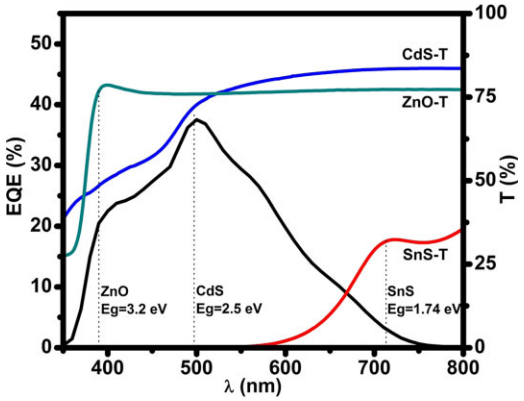

Figure 7 External quantum efficiency (EQE, dark line) of the solar cell and the optical transmittance (T) of the component films of the cell; wavelengths corresponding to the E_g are indicated.

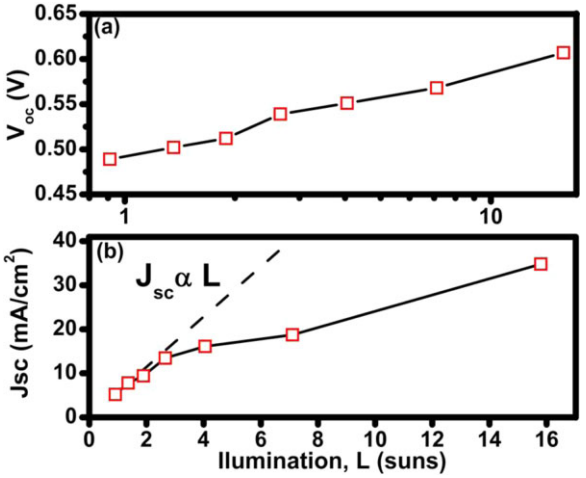

Figure 8 (a) Open-circuit voltage (V_{oc}) and (b) short-circuit current density (J_{sc}) of the solar cell measured in the exterior under solar radiation intensity of 1–16 suns; the dotted line indicates linear variation of J_{sc} with intensity of illumination (L).

SnS-CUB, CdS, and ZnO films. The wavelength corresponding to their E_g is indicated. EQE values stay low throughout the red region, and do not rise sharply at wavelengths shorter than the threshold for SnS-CUB. Thus, the quality of the material has to improve which will enhance the free carrier lifetime. Photocarrier generation in the cell sets-in at a wavelength 760 nm (photon energy 1.63 eV), instead of being closer to 715 nm corresponding to the E_g of SnS-CUB. It is possible that an interfacial layer is created on the stainless steel substrate during the initial phase of deposition of the SnS-CUB film in the chemical bath containing thioacetamide. A drop in EQE exists at wavelengths shorter than 496 and 388 nm, corresponding to the optical absorption thresholds in the CdS and ZnS films, respectively. Thus, the optical absorption in these films does not lead to carrier collection across the cell. Maximum EQE is only 37%, compared to nearly double this in SnS-ORT cells with η in the 3.8–4.6% range [4, 5]. A quick thought might be to combine SnS-CUB with SnS-ORT in order to increase the optical absorption. In solar cell structures of that type: SnO_2:F/CdS/SnS-CUB (100 nm)/SnS-ORT-Ag, V_{oc} was found to increase from 0.350 to 0.370 V; J_{sc} from 0.76 to 1.23 mA cm^{-2} V and η from 0.11 to 0.2% as the SnS-ORT thickness increased from 250 to 550 nm [7]. Thus, such effort must also seek to improve the crystalline grain diameters of both components through heating, such as in an appropriate ambient to promote grain growth, but without loss of S [5]. Previous attempt to combine the films without such heat treatment suggested that the approach is feasible, the addition of SnS-ORT to SnS-CUB improved the cell performance [7]. A limitation of chemically deposited SnS-ORT film is that it is less compact compared with SnS-CUB film [14, 17], which would be an aspect requiring attention while stacking SnS-CUB/SnS-ORT thin films.

8 Solar cell characteristics under sunlight

Figure 8(a) and (b) shows the variation in V_{oc} and J_{sc} of the cell measured outdoor with the data normalized for intensity of solar radiation of 1000 W m^{-2} near-mid day labeled as one sun. This measurement was done subsequent to measurements made indoor under standard conditions, given in Fig. 6. In an ideal solar cell, J_{sc} would vary linearly with solar radiation intensity and V_{oc} would vary logarithmically. However, a reduction in the shunt resistance at higher intensities increases the leakage current and leads to reduction in J_{sc}. In the present case, J_{sc} increases proportionately only up to 2.79 suns, and then suffers a reduction, as seen from the deviation of J_{sc} from the dashed line representing proportionality. At approximately 16 suns, J_{sc} is only about 35 mA cm^{-2} instead of being nearly 100 mA cm^{-2}. Increase in V_{oc} is nearly logarithmic. At one sun, V_{oc} is 0.482 mV, and at nearly 16 suns, it is 0.606 V.

The stability of these solar cells under solar radiation is attested by the J–V characteristics presented in Fig. 9, recorded subsequent to the measurements of J_{sc} and V_{oc} given in Fig. 8. In Table 1 are listed the cell parameters. Here, η has the best value of 1.28% for the measurement

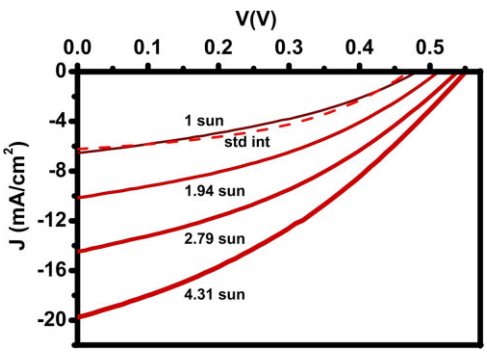

Figure 9 J–V characteristics of the cell measured under standard conditions in the interior (std int.) and those measured under solar radiation intensity (1 sun = 1000 W m^{-2}) of 1–4.31 suns.

Table 1 Summary of solar cell parameters determined from the data presented in Figs. 6, 8, and 9.

intensity (sun)	V_{oc} (V)	J_{sc} (mA cm^{-2})	FF	η (%)
1 (std int.)	0.470	6.23	0.44	1.28
1	0.482	6.55	0.36	1.14
1.94	0.512	10.14	0.38	1.00
2.79	0.539	14.48	0.37	1.03
4.31	0.551	19.76	0.35	0.91
7.11	0.568	18.75	–	–
15.8	0.607	34.8	–	–

made under standard conditions in the interior (std int.) mainly because of a higher fill factor (FF). Values of J_{sc} and V_{oc} increase under concentrated sunlight, even though the proportionality of J_{sc} with intensity is lost even at 1.96 suns: reaching only 10.14 and not 12.7 mA cm^{-2}. What is important here is that these solar cells remain stable in repeated measurements after having gone through measurements under concentrated light.

9 SnS-CUB and SnS-ORT: distinct semiconductors of the same chemical compound Even though the chemical substance of SnS-CUB presented here is the same as the more common SnS-ORT, the physical characteristics of these two semiconductors are very distinct [32]. Thin films of SnS-CUB are very compact, but of SnS-ORT are less so. So far SnS-CUB has been obtained only by chemical deposition or successive ion-layer adsorption and reaction (SILAR) under specific conditions [9, 14, 17], whereas SnS-ORT are obtained by a variety of physical and chemical techniques and it occurs in nature as mineral herzenbergite [15–17]. Formation of SnS-CUB nanocrystals too requires a chemical method [13], and its mineral form is not yet known. The optical band gap of SnS-CUB is nearly 1.7 eV (direct-forbidden), whereas it is notably different 1.1 eV (indirect) for the more common SnS-ORT, when both are prepared by chemical deposition [32]. The electrical conductivity in the dark for chemically deposited SnS-ORT is typically 20 times more than that of SnS-CUB. Heating a film of SnS-ORT of 300 nm in thickness at 300 °C in nitrogen leads to an increase in the electrical conductivity from 1.4×10^{-6} to $2 \times 10^{-4}\,\Omega^{-1}\,\mathrm{cm}^{-1}$, where as the electrical conductivity remains essentially the same at $6 \times 10^{-8}\,\Omega^{-1}\,\mathrm{cm}^{-1}$ for SnS-CUB thin film. In a thicker SnS-CUB film (550 nm instead of 300 nm in Ref. [32]) as reported in the present work, the dark conductivity is 2.5 times this value, $0.22 \times 10^{-6}\,\Omega^{-1}\,\mathrm{cm}^{-1}$. In both materials, the electrical conductivity increases by one to two orders of magnitude under an intensity of illumination of 850 W/m^2 [32]. The compact nature of the SnS-CUB film makes it very stable under heating in air at temperatures up to 300 °C; it would require heating in air at 550 °C for 2 h and 30 min to convert an SnS-CUB film of 300 nm thickness totally to SnO_2 [9]. For a SnS-ORT film of 750 nm thickness, heating in air at 500 °C for 30 min would convert it to SnO_2; and the conversion does occur at 400 °C as well during 3 h [16]. The formation of a stratified compact layer of n-SnO_2 produced over SnS-CUB during heating in air would in itself make a p–n junction [9], but such effect has not been reported in SnS-ORT. Thus, the availability of SnS-CUB and SnS-ORT offers many options for solar cell designs.

10 Conclusions We reported here a solar cell structure using a thin film SnS-CUB absorber with conversion efficiency of 1.28% and a V_{oc} of 0.470 V. The crystalline structure of SnS-CUB absorber film used here fits well a cubic unit cell of cube-edge 1.159 nm. The optical band gap of the material is 1.74 eV and the estimated light generated current density in the cell should reach 18.2 mA cm^{-2}. However, J_{sc} of the solar cell is one-third of this. Photoconductivity response studies suggested that the life time of photo-generated carriers in the absorber material is 2–20 ns, which leads to their insufficient separation and collection before recombination. This aspect is illustrated by the EQE curve, which reaches a maximum value of 37% for a wavelength of light 500 nm, but falls-off steeply at longer and shorter wavelengths. The crystalline grain size of the material is 24 nm, which need to be increased further to enhance the carrier lifetime and hence improve the cell performance. This may be achieved by heating the SnS-CUB film in an appropriate ambient and temperature for optimum duration. Measurement of the solar cell under sunlight testifies to the stable performance of the cell. Thus, it is worthwhile to investigate this solar cell structure further.

Acknowledgements We are grateful to Maria Luisa Ramón García for the XRD measurements and to José Escorcia García for outdoor J–V measurements. Financial support for this work was received from PAPIIT-UNAM IN117912, IN116015, and IT100814; and from CONACYT-LIFYCS and CeMIE-Sol-35. ARGA acknowledges CONACyT (MEXICO) for graduate fellowship.

References

[1] L. M. Peter, Phil. Trans. R. Soc. A **369**, 1840 (2011).
[2] S. Abermann, Sol. Energy **94**, 37 (2013).
[3] I. L. Repins, M. J. Romero, J. V. Li, Su-Huai Wei, D. Kuciauskas, C.-S. Jiang, C. Beall, C. DeHart, J. Mann, W.-C. Hsu, G. Teeter, A. Goodrich, and R. Noufi, IEEE J. Photovolt. **3**, 439 (2013).
[4] V. Steinmann, R. Jaramillo, K. Hartman, R. Chakraborty, R. E. Brandt, J. R. Poindexter, Y. S. Lee, L. Sun, A. Polizzotti, H. H. Park, R. G. Gordon, and T. Buonassisi, Adv. Mater. **26**, 7488 (2014).
[5] P. Sinsermsuksakul, L. Sun, S. W. Lee, H. H. Park, S. B. Kim, C. Yang, and R. G. Gordon, Adv. Energy Mater. **4**, 1400496 (1–7) (2014).
[6] M. T. S. Nair, E. Barrios-Salgado, A. R. Garcia, M. R. Aragón-Silva, J. Campos, and P. K. Nair, ECS Trans. **41**, 177 (2011).
[7] D. Avellaneda, M. T. S. Nair, and P. K. Nair, Thin Solid Films **517**, 2500 (2009).

[8] E. Barrios-Salgado, M. T. S. Nair, and P. K. Nair, ECS J. Solid State Sci. Technol. **2**, Q169 (2014).
[9] D. Avellaneda, M. T. S. Nair, and P. K. Nair, J. Electrochem. Soc. **155**, D517 (2008).
[10] M. T. S. Nair, P. K. Nair, R. A. Zingaro, and E. A. Meyers, J. Appl. Phys. **75**, 1557 (1994).
[11] R. González-Lúa, J. Escorcia-García, D. Pérez-Martínez, M. T. S. Nair, J. Campos, and P. K. Nair, ECS J. Solid State Sci. Technol. **4**, Q9 (2015).
[12] A. N. Mariano and K. L. Chopra, Appl. Phys. Lett. **10**, 282 (1967).
[13] E. C. Greyson, J. E. Barton, and T. W. Odom, Small **2**, 368 (2006).
[14] C. Gao, H. Shen, L. Sun, and Z. Shen, Mater. Lett. **65**, 1413 (2011).
[15] M. T. S. Nair and P. K. Nair, Semicond. Sci. Technol. **6**, 132 (1991).
[16] P. K. Nair, M. T. S. Nair, R. A. Zingaro, and E. A. Meyers, Thin Solid Films **239**, 85 (1994).
[17] A. R. Garcia-Angelmo, M. T. S. Nair, and P. K. Nair, Solid State Sci. **30**, 26 (2014).
[18] L. A. Burton and A. Walsh, J. Phys. Chem. C **116**, 24262 (2012).
[19] A. J. Biacchi, D. D. Vaughn II, and R. E. Schaak, J. Am. Chem. Soc. **135**, 11634 (2013).
[20] A. Rabkin, S. Samuha, R. E. Abutbul, V. Ezersky, L. Meshi, and Y. Golan, Nano Lett. **15**, 2174 (2015).
[21] D. K. Schröder, Semiconductor Material and Device Characterization (Wiley, New York, 2006).
[22] M. Parenteau and C. Carlone, Phys. Rev. B **41**, 5227 (1990).
[23] G. L. Araújo and A. Marti, Sol. Energy Mater. Sol. Cells **33**, 213 (1994).
[24] J. Nelson, The Physics of Solar Cells (Imperial College Press, London, 2003).
[25] G. Nair, L.-Y. Chang, S. M. Geyer, and M. G. Bawendi, Nano Lett. **11**, 2145 (2011).
[26] J. B. Johnson, H. Jones, B. S. Latham, J. D. Parker, and R. D. Engelken, Semicond. Sci. Technol. **14**, 501 (1999).
[27] N. M. Mangan, R. E. Brandt, V. Steinmann, R. Jaramillo, J. V. Li, J. R. Poindexter, K. Hartman, L. Sun, R. G. Gordon, and T. Buonassisi, 40th IEEE Photovoltaic Specialist Conference (PVSC), 8–13 June 2014 (Golden, CO), pp. 2373–2378, doi: 10.1109/PVSC.2014.6925404.
[28] M. Ichimura, Sol. Energy Mater. Sol. Cells **93**, 375 (2009).
[29] L. A. Burton and A. Walsh, Appl. Phys. Lett. **102**, 132111(1–3) (2013).
[30] P. Sinsermsuksakul, K. Hartman, S. B. Kim, J. Heo, L. Sun, H. Hejin Park, R. Chakraborty, T. Buonassisi, and R. G. Gordon, Appl. Phys. Lett. **102**, 053901(1–5) (2013).
[31] T. Ikuno, R. Suzuki, K. Kitazumi, N. Takahashi, N. Kato, and K. Higuchi, Appl. Phys. Lett. **102**, 193901(1–4) (2013).
[32] D. Avellaneda, G. Delgado, M. T. S. Nair, and P. K. Nair, Thin Solid Films **515**, 5771 (2007).

